Received: 18 January 2017 | Revised: 28 February 2017 | Accepted: 6 March 2017

DOI: 10.1002/aoc.3826

FULL PAPER

WILEY Applied Organometallic Chemistry

A versatile synthesis of arylaminotetrazoles by a magnetic Fe@Phendiol@Mn nano-particle catalyst and its theoretical studies

Davood Habibi | Somayyeh Heydari | Mina Afsharfarnia | Zahra Rostami

Department of Organic Chemistrty, Faculty of Chemistry, Bu-Ali Sina University, Hamedan 6517838683, Iran

Correspondence
Davood Habibi, Department of Organic Chemistrty, Faculty of Chemistry, Bu-Ali Sina University, Hamedan, 6517838683 Iran.
Email: davood.habibi@gmail.com

The Fe_3O_4 magnetic nano-particles were modified with 1,10-phenanthroline-5,6-diol and the relevant Mn complex (Fe@Phendiol@Mn) synthesized as a nano-magnetic heterogeneous catalyst to be used for the synthesis of various arylaminotetrazoles from various arylcyanamides and sodium azide in DMF at 120 °C. Also, the nano-catalyst characterized by different methods such as the elemental analysis (CHN), ICP, FT-IR, XRD, EDX, SEM, TEM, TG-DTA, VSM and XPS. In addition, the theoretical study of the Fe@Phendiol@Mn nano-catalyst was performed using the Gausian software. The calculated results showed that the Gibbs free energy and the standard enthalpy values are negative; therefore the complex is stable. Incidentally, the computational chemistry descriptions including the electronic chemical potential, global hardness, electrophilicity index, energy gap, global softness and electronegativity were calculated.

KEYWORDS

1,10-Phenanthroline-5,6-diol, arylaminotetrazoles, Fe_3O_4 magnetic nano-particle, heterogeneous catalyst, Mn complex, theoretical study

1 | INTRODUCTION

Tetrazoles have several applications in biological and pharmaceutical industries,[1–3] due to their antiallergic and anti-asthmatic,[4] antiviral and anti-inflammatory,[5] anti-neoplastic,[6] and cognition disorder activities.[7] Tetrazoles were used as explosives and rocket propellants,[8–10] and applied in coordination chemistry,[11–13] preparation of imidoylazides,[14] and also in agriculture farms as plant growth regulators, herbicides, and fungicides stabilizers.[15–17] So, the chemistry of tetrazoles has gained increasing attention since the early 1980s.[18] The anionic tetrazoles are almost ten times more lipophilic than corresponding carboxylates, which is an important factor for designing drug molecules to pass through the cell membranes.[19] There are several methods for preparation of tetrazoles, for example addition of the azide anion to nitriles, cyanates and cyanamides which is the most common route for preparing 5-substituted tetrazoles, 5-aryl/alkyl oxytetrazoles and 5-aryl/alkyl aminotetrazoles, respectively.[20–26] Also, cyanamides may be converted to aminotetrazoles using hydrazoic acid, which often result in a mixture of isomers.[27]

In addition, 5-monosubstituted-amino-1*H*-tetrazoles were synthesized by thermal isomerization of 1-substituted-5-amino-1*H*-tetrazoles in boiling ethylene glycol or melt.[28,29]

Another possible method of obtaining the 5-monoalkylaminotetrazoles was an adaption of the von Braun degradation of tertiary amines with cyanogens bromide. In this way, it might be possible to eliminate an alkyl group from a 5-dialkylamino-tetrazoles.[30,31]

These methods suffer from one or more disadvantages, such as low yield, long reaction times, harsh reaction conditions, difficult obtaining and/or preparation of starting materials, use of expensive and toxic reagents, and the in situ generation of hydrazoic acid which is highly toxic and explosive.[32–36]

Congreve has reported a two-step synthesis of 1-aryl-5-amino-1*H*-tetrazoles from the corresponding 1-aryltetrazoles via cyanamide intermediates.[37] Vorobiov and co-workers

published a three-step synthesis of 1-aryl-5-amino-1*H*-tetrazoles in low yields from the corresponding aromatic amines via isolation of cyanamide intermediates.[38]

Incidentally, several regiospecific syntheses of arylaminotetrazoles have been reported through the [3 + 2] cycloaddition of cyanamides using NaN_3 in the presence of catalysts such as $ZnCl_2$,[39] $AlCl_3$[40] and Iranian natrolite zeolite.[41] $ZnCl_2$ and $AlCl_3$ are homogeneous catalysts which are very difficult to be separated from the reaction mixture. Thus, development of the useful catalytic systems for tetrazole synthesis still remains as active research area. Industry favors application of heterogeneous catalysts over homogeneous processes in view of the ease of handling, simple work-up, and separations.[42]

Among catalysts, application of the nano-catalysts has received considerable attention in recent decades as heterogeneous catalysts for organic synthesis due to their unique physical surfaces and catalytic properties.[43,44]

The surface area to volume ratio increases with the decrease in radius of the sphere and vice versa. Therefore as particle size decreases, a greater portion of the atoms are found at the surface compared to those inside. Thus, nanoparticles have a much greater surface area per unit volume compared with the larger particles.

Also, as growth and catalytic chemical reaction occurs at surfaces, therefore a given mass of nano-material will be much more reactive than the same mass of material made up of large particles.

So, we interested to design the Mn nano-catalyst with better reactivity compared to the pure Mn(II)(Phendiol) complex, and hereby would like to report application of the Fe@Phendiol@Mn nano-catalyst for the one-pot two-component selective synthesis of various arylaminotetrazoles (**A.** or **B**) from different arylcyanamides with sodium azide in DMF at 120 °C (Scheme 1).

2 | EXPERIMENTAL

2.1 | Synthesis of a Fe@Phendiol@Mn nano-catalyst

2.1.1 | Stage 1: General procedure for preparation of Fe_3O_4 magnetic nano particles (Fe_3O_4 MNPs)

The Fe_3O_4 MNPs was prepared according to the literature.[45] Briefly, the mixture of $FeCl_3.6H_2O$ (11.44 g) and

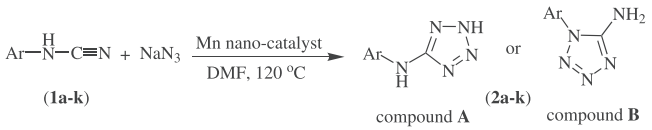

SCHEME 1 Synthesis of arylaminotetrazoles

$FeCl_2.4H_2O$ (4.3 g) was dissolved in water (100 ml), and the solution stirred for 0.5 h in 80 °C. The solution of 37% ammonia was then added dropwise with vigorous stirring which a black solid product obtained when a reaction media reached to pH 10. The mixture was heated for 0.5 h at 70 °C and the black solid product filtered, washed with water (3 × 20 ml) and dried at 80 °C for 12 h.

2.1.2 | Stage 2: Synthesis of a ligand

First: Synthesis of 1,10-phenanthroline-5,6-dione

1,10-Phenanthroline-5,6-dione was prepared according to the literature.[46] Briefly, an ice cold mixture of concentrated H_2SO_4 (40 ml) and HNO_3 (20 ml) was added to 1,10-phenanthroline (4.0 g, 22.2 mmol) and KBr (4.0 g, 33.6 mmol). The mixture was heated at reflux for 4 h. The hot yellow solution was poured over ice (500 ml) and neutralized carefully with NaOH until neutral to slightly acidic pH. Extraction with $CHCl_3$ followed by drying with Na_2SO_4 and removal of solvent gave 4.5 g (96%) of 1,10-phenanthroline-5,6-dione.

Second: Synthesis of 1,10-phenanthroline-5,6-diol (Phendiol)

1,10-Phenanthroline-5,6-diol was prepared according to the literature.[47] Briefly, a mixture of 1,10-phenanthroline-5,6-dione (0.70 g, 3.33 mmol) and rubeanic acid (dithiooxamide, 0.480 g, 3.99 mmol) was refluxed in ethanol (25 ml) for 16 h. Upon cooling of the reaction mixture to room temperature, the yellow-brown precipitate was separated by filtration, washed with ethanol (20 ml) and dried in Vacuo.

2.1.3 | Stage 3: Surface modification of Fe_3O_4 MNPs with Phendiol (Fe@Phendiol)

Surface modification of Fe_3O_4 MNPs with Phendiol was preformed according to the literature.[45] Briefly, Fe_3O_4 MNPs prepared from the stage one (0.5 g) were dispersed in water/ethanol solution (50 ml, 1:1) by sonication at room temperature for 20 min. Then, Phendiol prepared from the stage two (0.25 g, 1.8 mmol) dissolved in ethanol (5 ml) was added and placed under ultrasound for 3 hours. Fe@Phendiol was separated by external magnet, washed with ethanol (20 ml) and dried under vacuum at 50 °C for 2 h.

2.1.4 | Stage 4: General procedure for preparation of the Fe@Phendiol@Mn nano-catalyst

The Mn nano-catalyst was prepared according to the literature.[45] Briefly, Fe@Phendiol prepared from the stage three (0.2 g) and $Mn(CH_3COOH)_2.4H_2O$ (0.735 g, 3 mmol) were mixed in ethanol (30 ml) and placed in an ultrasonic bath for 3 h at room temperature. The resulting catalyst was

separated with an external magnet, washed with ethanol (20 ml), dried in vacuum at 70 °C for 6 h, and kept in a desiccator.

2.2 | Apparatus and reagents

The IR spectra (KBr) were recorded on Perkin–Elmer GX Fourier transform infrared spectrometer (FT-IR). The NMR spectra were recorded on a Bruker Ultra-Shield 500 spectrometer. The TEM images were recorded on a Zeiss-EM10C-80 KV transmission electron microscope, and the SEM images were recorded on a Philips XL-30 scanning electron microscope. The XRD measurements were done by a Bruker D8 Advance powder diffractometer, using Cu Kα (λ = 1.54 A°) as the incident radiation.

For counting the nanoparticles, size distributions were measured by the Zetasizer Nano-ZS-90 (ZEN 3600, MALVERN) instrument. In addition, the ICP measurements for the metal content evaluation were performed using a Perkin-Elmer ICP/6500. Magnetic measurements were carried out using an Iranian Meghnatis Daghigh Kavir Co. The chemical surface composition of the Mn complex was determined by XPS (BesTec, Germany).

Chemicals and solvents were purchased from the Merck and Aldrich chemical companies and used without further purification.

2.3 | Stage 5: Application of the Mn nano-catalyst for preparation of various arylaminotetrazole

A mixture of arylcyanamide (2 mmol), sodium azide (0.195 g, 3 mmol), and the Fe@Phendiol @Mn nano-catalyst (50 mg) was stirred at 120 °C in DMF (10 ml) until the TLC monitoring showed no further progress in the conversion. When the reaction mixture came to room temperature, the nano-catalyst was separated by a strong magnet, 4 N HCl (20 ml) and ethyl acetate (35 ml) were added to the filtrate and the organic layer extracted with decanting. The aqueous layer was washed with ethyl acetate (2 x 25 ml) and the organic layers combined. The resulting solution was then dried over anhydrous $MgSO_4$, the solvent evaporated and the resulting solid recrystallized in ethanol.

3 | RESULTS AND DISCUSSION

3.1 | Synthesis of a Fe@Phendiol@Mn nano-catalyst

Synthesis of a Fe@Phendiol@Mn nano-catalyst was carried out via the four stages which were comprehensively described in the experimental section (Scheme 2):

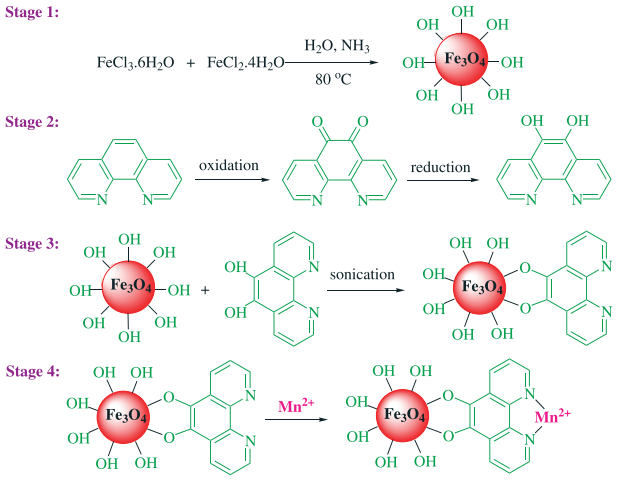

SCHEME 2 Schematic synthesis of the Fe@Phendiol@Mn nano-catalyst

3.2 | Characterization of a Fe_3O_4 MNPs@Phendiol@Mn nano-catalyst

Formation of the Fe@Phendiol@Mn nano-catalyst was verified using the CHN analysis, FT-IR, X-ray diffraction (XRD), dispersive X-ray spectroscopy (EDX), scanning electron microscope (SEM), transmission electron microscope (TEM), thermogravimetry-differential thermal analysis (TG-DTA), vibrating sample magnetometer (VSM) and XPS (X-ray photoelectron spectroscopy).

3.2.1 | Characterization of the nano-catalyst by the elemental analysis (CHN)

The elemental analysis report for C, H and N, and the ICP information for Mn are presented in Table 1. These data indicated the fact that the CHN content increased with increasing the Phendiol ligand attached to the surface of Fe_3O_4 MNPs. The loading of Mn was determined by the EDX analysis and the ICP information which the final Mn content measurement was around 0.43 mmol/g, indicating that %54.7 of the Phendiol ligands were complexed with the Mn ions.

3.2.2 | Characterization of the nano-catalyst by the IR spectroscopy

Figure 1 shows the three FT-IR spectra of: Fe_3O_4 MNPs (blue), Fe@Phendiol (green), and Fe@ Phendiol@Mn (red). Fe_3O_4 MNPs exhibits basic characteristic peak at approximately 580 cm^{-1} which is attributed to the presence of the Fe–O stretching vibrations. The FT-IR spectrum of Fe@Phendiol shows several original signals located at the 3020–3066 cm^{-1} (C-H of the pyridine ring), the peaks at 1434–1437 cm^{-1} (C = C of the pyridine ring) and 1670 (C = N of the Phendiol ligand). It could be concluded from the above results that the Fe_3O_4 MNPs was modified

TABLE 1 Chemical composition of the immobilized Mn nano-catalyst on the Fe_3O_4

No	Sample	CHN analyses (wt%) C	N	Mn	Fe@Phendiol (g/mmol)	Fe@Phendiol@Mn (g/mmol)	% of coordinated ligand to Mn^{2+}
1	Fe_3O_4 MNPs	–	–	–	–	–	–
2	Fe@Phendiol	24.65	1.05	–	1.05 ÷ 14 = 0.075 x 10 (since we took 0.1 g for CHN) = 0.75	–	–
3	Fe@Phendiol@Mn	19.11	0.11	1.83	0.11 ÷ 14 = 0.00786	0.43 (from ICP)	0.43 ÷ 0.00786 = 54.70

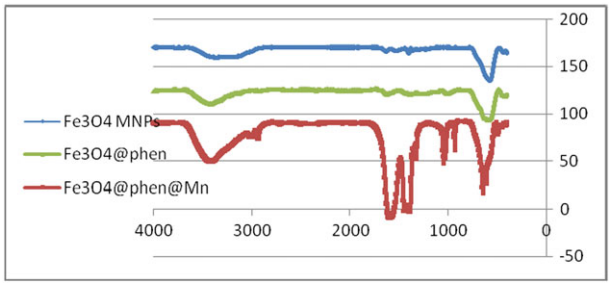

FIGURE 1 The IR spectra of Fe_3O_4 MNPs (blue), Fe@Phendiol (green), and the Fe@Phendiol@Mn nano-catalyst (red)

successfully. Comparison of the two IR spectra (blue and green) confirms anchoring of the Phendiol ligand on the surface of the magnetic nanoparticles. Furthermore, after complexing of Mn with Fe@Phendiol, the weak absorption peak at 413 cm^{-1} was appeared which is attributed to the Mn-N bands.

3.2.3 | Characterization of the catalyst by the XRD patterns

In addition, the crystalline phase and purity of the synthesized material was determined by the XRD patterns (Figure 2). The particle size was calculated by means of the Debye Scherrer formula based on the full width at half-maximum of the highest intensity diffraction peak at 2θ = 35.6° and was found to be about 18 nm. The XRD pattern exhibited peaks at 2θ of 31, 35, 43, 54, 57 and 62.5 correspond to the spinal structure of Fe_3O_4 MNPs which attributed to (2 2 0), (3 1 1), (4 0 0), (4 2 2), (5 1 1) and (4 4 0) faces of crystal. The diffraction peaks in this pattern can be well indexed to the cubic spinel phase of Fe_3O_4 MNPs (Figure 2, blue). The XRD pattern of the Fe@Phendiol@Mn nano-catalyst exhibited broadened pattern due to its non-crystalline nature at 2θ = 15–30 and also 30.2, 35.6, 43.3, 53.6, 57.3 and 62.8 which corresponded to the Mn catalyst structure (Figure 2, red). Finally, the XRD patterns represent similar diffraction peaks which indicate that the coating agent does not significantly affect the crystal structure of the magnetite nanoparticles, and the Fe_3O_4 MNPs particles were successfully coated with the ligand.

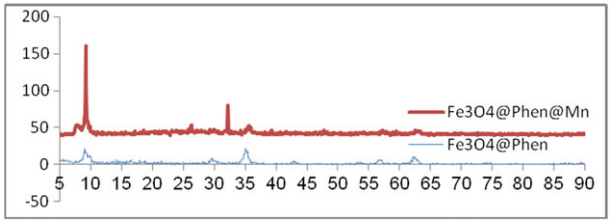

FIGURE 2 The XRD patterns of Fe_3O_4 MNPs (blue), and the Fe@Phendiol@Mn nano-catalyst (red)

3.2.4 | Characterization of the nano-catalyst by the EDX analysis

The chemical composition of the Fe@Phendiol@Mn nano-catalyst was determined by the EDX analysis (Figure 3). The survey scan provided the presence of the anticipated elements in the structure of the nano-catalyst, namely iron, oxygen, nitrogen, manganese and carbon.

3.2.5 | Characterization of the nano-catalyst by the SEM and the TEM images

The morphology and the particle size distribution of the Fe@Phendiol@Mn catalyst were determined by the SEM and TEM images (Figure 4 and 5). According to these figures, the nanoparticles appearance and their sizes are similar, indicating that the Fe@Phendiol@Mn nano-catalyst have good mechanical stability and have not been destroyed during the whole modification.

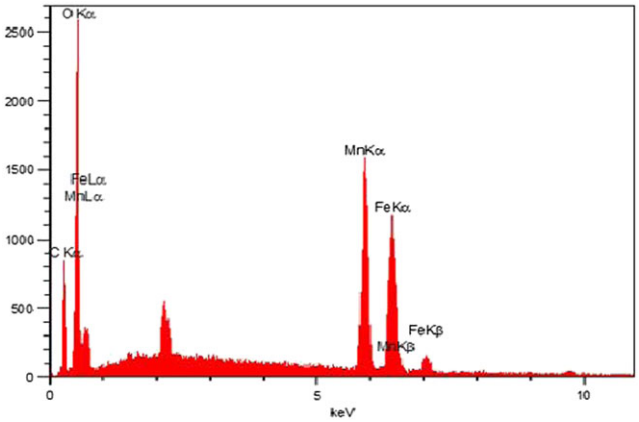

FIGURE 3 The EDX analysis of the Fe@Phendiol@Mn nano-catalyst

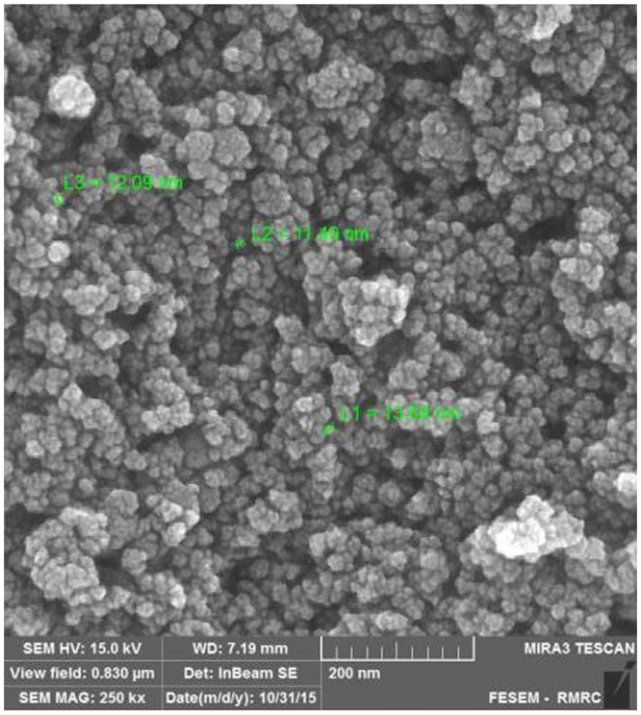

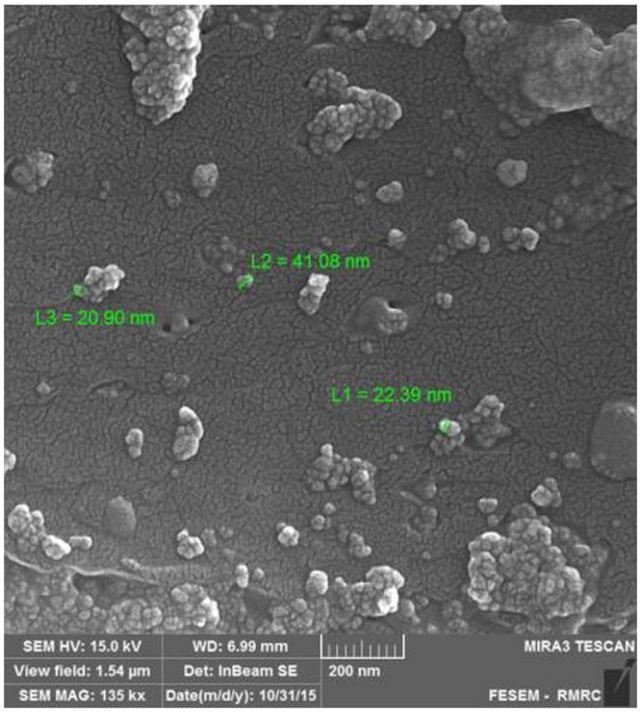

FIGURE 4 The SEM images of Fe@Phendiol (left) and the Fe@Phendiol@Mn nano-catalyst (right)

According to the nanoparticle size and the ligand capping to prevent any agglomeration, the Fe@Phendiol@Mn nano-catalyst could be used as a suitable catalyst for the synthesis of various tetrazoles. However, the presence of Mn ions in the Fe@Phendiol@Mn nano-catalyst purposely coated to increase the electrical conduction and hence to improve the quality of the SEM micrographs.

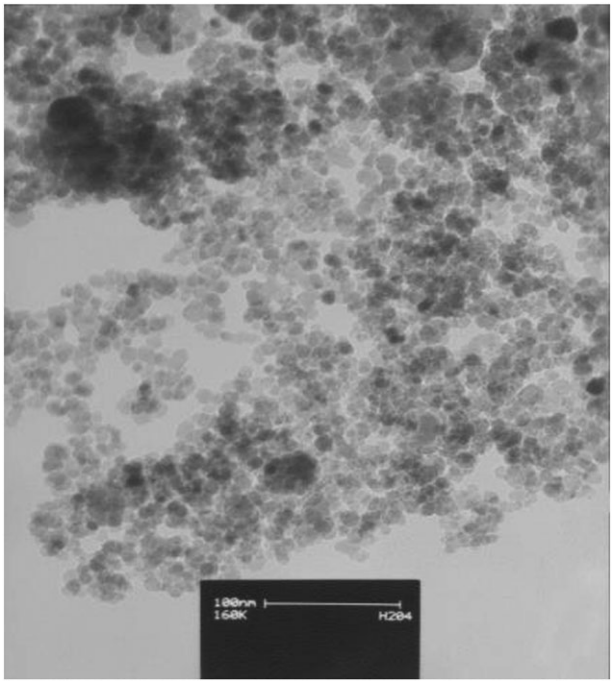

FIGURE 5 The TEM images of the Fe@Phendiol@Mn nano-catalyst

3.2.6 | Characterization of the nano-catalyst by the TG-DTA technique

The thermogravimetric analysis curves of the Fe@Phendiol@Mn nano-catalyst show the mass loss of the organic materials as they decompose upon heating (Figure 6). It can be observed that the nano-catalyst shows two weight loss steps in the temperature range of the DTG analysis. The initial weight loss at 200–220 °C is probably due to the complex decomposition, and the second step at about 320 °C is contributed to the thermal decomposition of the coated layer in the nano-catalyst.

On the basis of these results, the well grafting of ligand groups on the support is verified and indicated that the nano-catalyst has a good thermal stability which is probably due to the strong interaction between the Phendiol ligand and Fe_3O_4 MNPs.

3.2.7 | Characterization of the catalyst by the VSM technique

The VSM analysis of Fe@Phendiol (Figure 7, left) and the Fe@Phendiol@Mn nano-catalyst (Figure 7, right) were performed in order to demonstrate their magnetic properties. As can be seen, both have magnetic properties, however, magnetization of the Fe@Phendiol@Mn nano-catalyst was decreased to some extent in comparison with Fe@Phendiol. This can be explained by considering the reduction in the dipolar–dipolar interactions between the magnetic

nanoparticles after their modification with the Phendiol ligand and complexation with the Mn ions which cause the more coating of Fe_3O_4 MNPs.

3.2.8 | Characterization of the nano-catalyst by the XPS spectroscopy

The XPS spectrum relating to the core level presence of the Mn 2p is shown in Figure 8. The binding energy shows two peaks at 644.0 and 653.2 eV which are attributed to the presence of the Mn 2p3/2 and Mn 2p1/2, respectively. These data confirm the formation of the Fe@Phendiol@Mn nano-catalyst as well as the Mn(II) oxidation state.[48]

It should be noted that from the XPS spectrum, not only the presence of Mn was concluded, but also we concluded the structure of the complex due to the oxidation state of Mn. We did not know which structure the Mn complex had, structure **A**, or **B**. The oxidation state of Mn(II) showed us that the structure **A** is correct, not **B**.

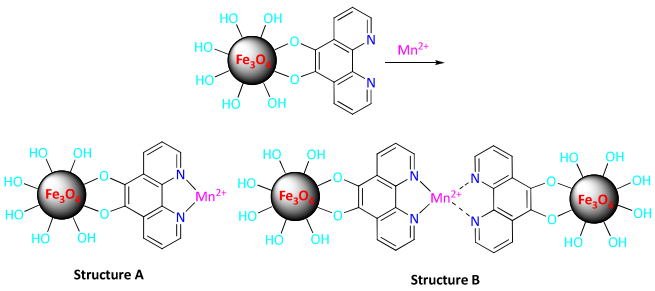

3.3 | Optimization of the reaction conditions

Most cyclization reactions are carried out in high temperatures and most organic solvents are not stable at these temperatures, so DMF was chosen as an optimum solvent. Then, the reaction of 2,5-dichlorophenylcyanamide (2 mmol) and sodium azide (3 mmol) was carried out as a model reaction in different temperatures and the optimum temperature was about 120 °C. The results showed that the reaction is specific in the presence of the Mn complex, since only the product **A** or **B** were obtained, while with the other reagents, the mixture of products (**A** + **B**) produced (Table 2).[49]

Also, in the other series of experiments with the model reaction, different amounts of the catalyst were used which the 50 mg of the Mn nano-catalyst was an optimum amount (Entry 8). Further increasing of the catalyst concentration had no effect on the rate and yield. Also the reaction had no progress in the absence of the catalyst even after 4 h.

3.4 | Synthesis of arylaminotetrazole derivatives

According to the optimized reaction conditions, the synthesis of various arylaminotetrazole derivatives were carried out from the reaction of arylcyanamides (2.0 mmol) with sodium azide (3.0 mmol) in DMF at 120 °C by the application of Mn nano-catalyst (50 mg) (Table 3).

Also, in a new reaction, the pure Mn(II)(Phendiol) complex was applied for the synthesis of 1-(4-nitrophenyl)-1*H*–tetrazole-5-amine (**2a**) from the reaction of *N*-(4-nitrophenyl)cyanamide (**1a**) with sodium azide in DMF at 120 °C.

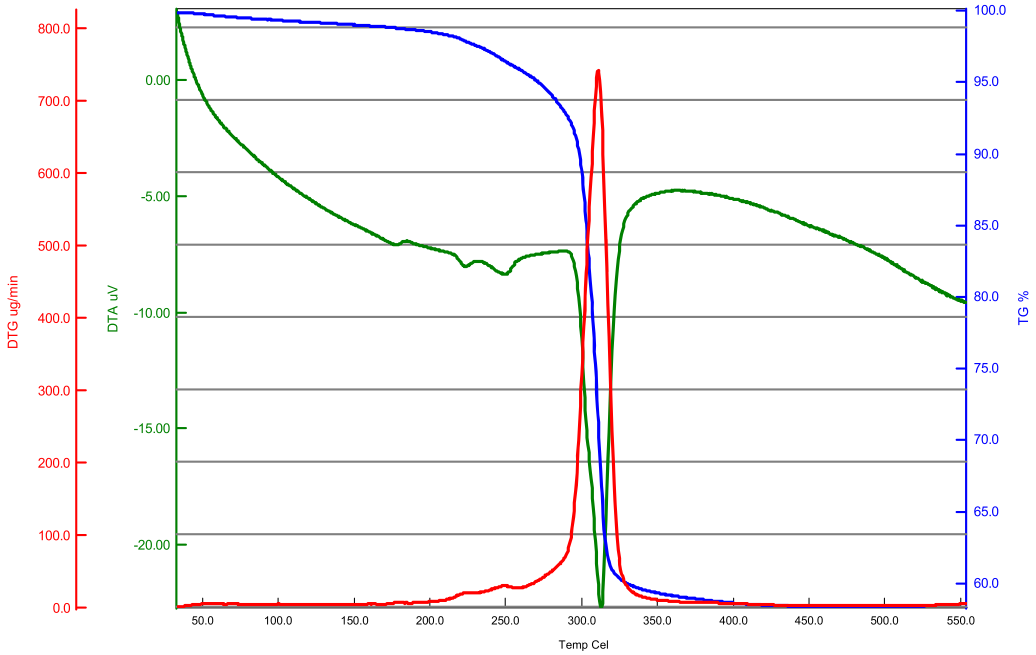

FIGURE 6 TG-DTA patterns of the Fe@Phendiol@Mn nano-catalyst in N_2 atmosphere

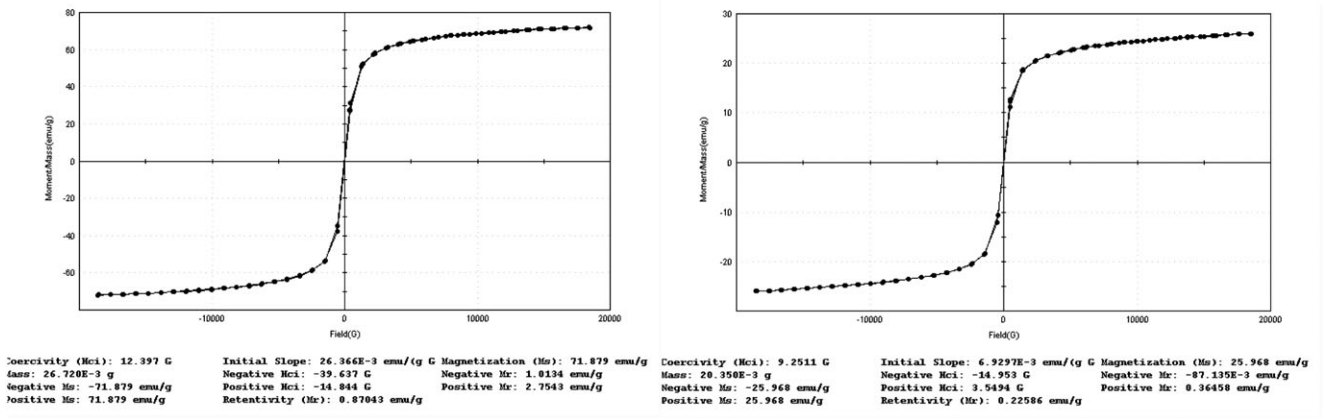

FIGURE 7 The VSM analysis of Fe@Phendiol (left), and the VSM analysis of the Fe@Phendiol@Mn nano-catalyst (right)

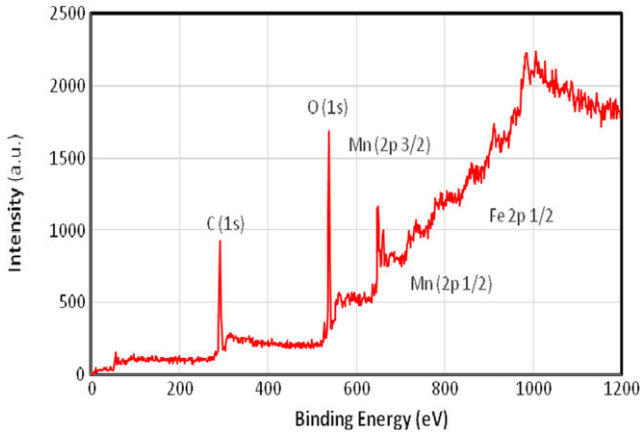

FIGURE 8 The XPS spectrum of the Mn(II) nano-catalyst

Interestingly, as we expected the reaction was completed with longer reaction time (235 min) and less yield (63%) compared with the application of the Mn nano-catalyst.

3.5 | Characterization of the arylaminotetrazole compounds

All known compounds were characterized by comparing their physical and spectral data with those reported in the literature. In the IR spectra of the 1-*H* substituted tetrazoles, the NH_2 peaks were disappeared and one strong absorptions band was detected (C-N stretching band,~ 1640–1690 cm^{-1}). The 1*H*–substituted tetrazoles are generally acidic substances and the relevant proton signal will be shifted to downfield, so the peak at $\delta = 7.80–8.30$ ppm can be attributed to the proton of the tetrazole ring.

3.6 | The catalyst reusability

Recovery of the catalyst is an important criterion because of the environmental and economical aspects, so the reusability of the Fe@Phendiol@Mn nano-catalyst was investigated as well. Therefore, the Mn nano catalyst was separated by filtration

TABLE 2 Comparison of different catalyst in the synthesis of arylaminotetrazoles at 120 °C

Entry	Catalyst	Solvent	Time (min)	Yield %	Product [49]
1	PPh_3	DMF	120	75	**A** + **B**
2	LiCl	DMF	100	70	**A** + **B**
3	SiO_2-$HClO_4$	Solvent-free	25	85	**A** + **B**
4	Al_2O_3-SO_3H	Solvent-free	30	86	**A** + **B**
5	$Fe(HSO_4)_3$	Solvent-free	30	90	**A** + **B**
6	Glacial HOAc	Glacial HOAc	30	87	**A** + **B**
7	Fe@Phendiol@Mn (140 mg)	DMF	100	77	**A** or **B**
8	Fe@Phendiol@Mn (50 mg)	DMF	85	80	**A** or **B**
9	Fe@Phendiol@Mn (50 mg)	DMSO	100	76	**A** or **B**
10	Fe@Phendiol@Mn (80 mg)	DMF	100	73	**A** or **B**
11	Fe@Phendiol@Mn (70 mg)	DMF	100	70	**A** or **B**
12	Fe@Phendiol@Mn (60 mg)	DMF	100	65	**A** or **B**

TABLE 3 Synthesis of arylaminotetrazoles in DMF at 120 °C

Entry	Cyanamide (1a–k)	Product (2a–k)	Time (min)	Yield (%)
1	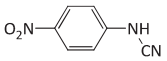	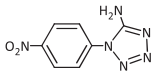	115	75
2	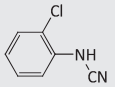	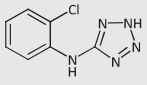	100	82
3	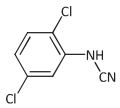	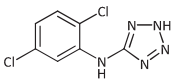	90	78
4	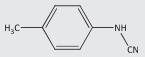	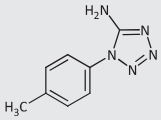	40	73
5	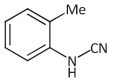	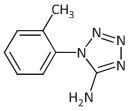	55	75
6	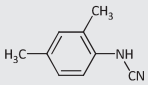	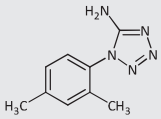	55	77
7	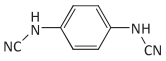	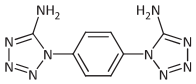	30	80
8	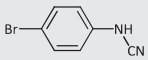	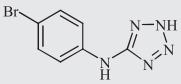	95	77
9	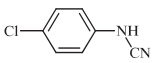	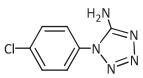	100	79
10	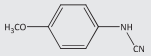	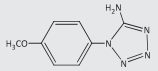	60	73
11	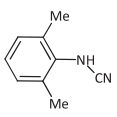	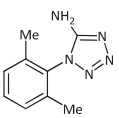	50	75

after the first run, washed with ethanol and dried at 120 °C under vacuum and then reused for the next successive runs under the same conditions (Scheme 3). No significant loss of the activity was observed, indicating that the Mn nano-catalyst is capable and has the high stability during the synthesis of various arylaminotetrazoles.

3.7 | Theoretical studies

All the atomic geometrical parameters of the structure were allowed to relax in the optimization at the density functional theory (DFT) level of B3LYP exchange-functional and 6-31G (d) standard basis set. For the Mn atom, the standard LANL2DZ basis set was used.[50] All of the calculations have been carried out using a locally modified version of the GAMESS electronic structure program.[51] The geometry optimization, natural bond orbital (NBO), density of state (DOS), highest occupied molecular orbital (HOMO) and lowest unoccupied molecular orbital (LUMO) were investigated, respectively. The energy difference between the HOMO and LUMO is termed as the HOMO–LUMO gap and also the density of state (DOS) plot was obtained from the Gauss Summ program. Dipole moment (μ), optimization energy (E_{opt}) and the point group of the Mn complex were obtained using the B3LYP/6-31G level.

By using the B3LYP/6-31G level, the obtained results for dipole moment (μ), optimization energy (E_{opt}) and the point group of the Mn complex are 2.6354, −1910.9720 and C1, respectively.

For the Mn complex, the computational chemistry descriptions[52,53] including the electronic chemical potential (μ), global hardness (η), electrophilicity index (ω),[54] energy gap (E_{gap}), global softness (s) and electronegativity (χ) were calculated by the following equations: [$\mu = -\chi = -(I + A)/2$], [$\eta = (I - A)/2$], [$\omega = \mu^{[2]}/2\eta$], and [$s = 1/2\eta$] where I ($-E_{HOMO}$) is the first vertical ionization energy and A ($-E_{LUMO}$) is the electron affinity of the Mn complex. The electrophilicity index is a measure of the electrophilic power of a molecule. The obtained results for I, A, E_{gap}, χ, η and s are −5.38852, −1.8028, −3.58573, −1.79286, 3.595658 and1.607178, respectively.

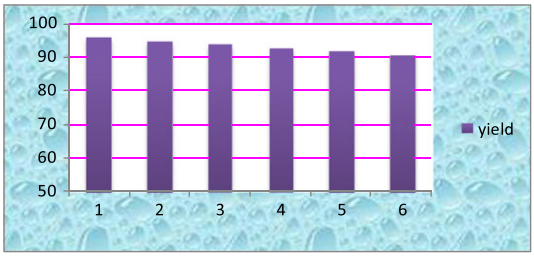

SCHEME 3 Reusability of the Fe@Phendiol@Mn nano-catalyst in the synthesis of arylaminotetrazoles

3.8 | Frequency calculations

The standard enthalpies (H) and the Gibbs free energy (G) values of the Mn complex were obtained by theoretical methods using the B3LYP/6-31G (d) level to obtain the minima of the potential energy. The calculated results show that both the Gibbs free energy [G (hartree) = −1910.8261] and the standard enthalpy [H (hartree) = −1910.7713] values are negative; therefore the complex is stable.

3.9 | Electrostatic potential maps

Electrostatic potential maps are especially useful for considering the charge redistribution, and changes in the reactive site, when molecules acquire and lose different functional groups. Molecular electrostatic potential (MEP) is capable of revealing the subtle changes observed in the spatial electronic distribution due to the changes in the molecular framework by locating and characterizing the critical points (CPs).[55] The MEP for the Mn complex which is in its optimized geometry was calculated using the Gauss view 5.0 W and sampled over the entire accessible surfaces of a molecule (corresponding to a van der Waals contact surface). This color coded surface provides information about the region of negative valued potential (deep green color), and the susceptible region (red color) likely to be attacked by nucleophiles. The topography map resulted from the MEP surface of the Mn complex has been shown in Scheme 4.

3.10 | Atomic and bonding properties

Natural bonding orbital (NBO) calculations are important for describing the charge transfer, and also for understanding the delocalization of the electron density between the filled (bonding (BD) or lone pair (LP)) Lewis type NBOs and the empty (antibonding and Rydberg) non-Lewis acceptor NBOs.

The interaction energy of filled and empty orbitals can be predicted by the second-order perturbation theory.[55] Also,

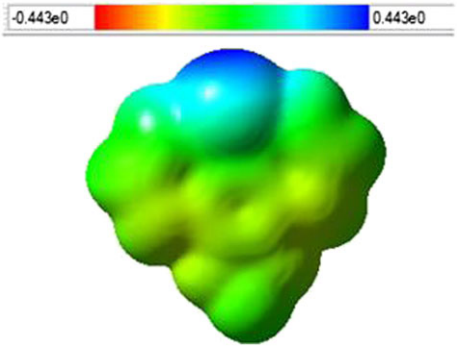

SCHEME 4 The molecular electrostatic potential surface of the Mn complex

for each donor $NBO_{(i)}$ and the acceptor $NBO_{(j)}$, the stabilization energy $E_{(2)}$ related to the electron delocalization i → j is estimated using the following equation[56]: $E_{(2)} = \Delta E_{i,j} = n_i [F_{i,j}^{[2]}/ (\varepsilon_i - \varepsilon_j)]$, where n_i is the donor orbital occupancy, ε_i and ε_j are the diagonal elements (orbital energies) and $F_{i,j}$ is the off diagonal NBO Fock matrix element. The larger interaction energy $E_{(2)}$ shows the stronger interaction between the electron donor atoms and the electron acceptor atoms. In this work, the NBO analysis was performed at the B3LYP/6-31G (d) level based on the stability energies $E_{(2)}$, occupation numbers and delocalization of the electron density for LP electrons of Mn atom for the most stable configuration. The results obtained in indicated that the total energy for the Mn LP (σ* or π*) delocalization increases with increasing the π character of the LP electrons of Mn for each donor acceptor atoms (Table 4). In addition, with increasing the π character.

of LP (Mn), there is decrease occupancy of the LP of Mn.

The DOS plots obtained from the Gauss Summ program for the Mn complex has been shown in Scheme 5. The big distance between the HOMO and LUMO levels indicates that the Mn complex is not a good conductive compound.

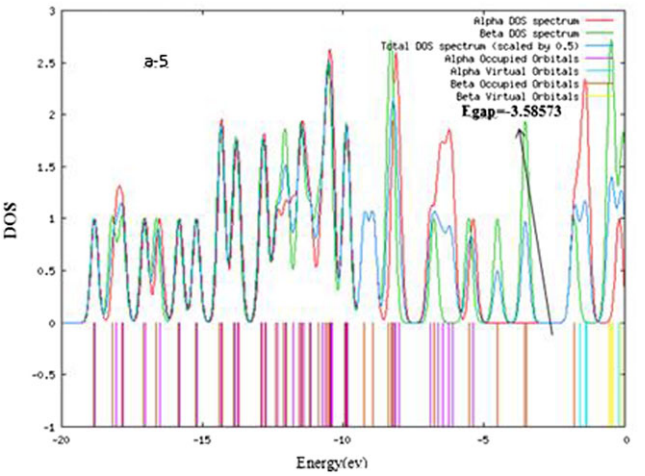

SCHEME 5 Optimized models for the stable configuration of the Mn complex and their DOS plots. Distances are in Å

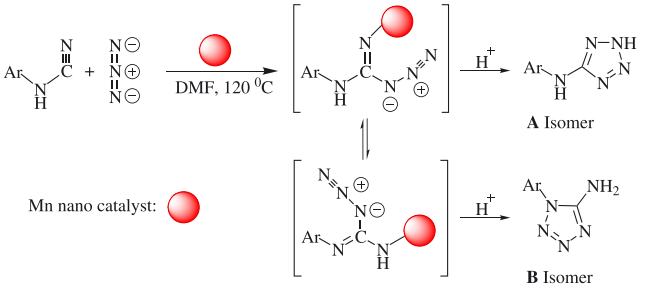

SCHEME 6 The plausible mechanism for the synthesis of different arylaminotetrazoles

3.11 | The plausible mechanism

The plausible mechanism for the synthesis of different arylaminotetrazoles is shown below (Scheme 6). The proposed mechanism is probably due to the Lewis acidity of the Mn nano-catalyst which can catalyze the cyclization reaction by activation of the C-N bond to produce the final product.

3.12 | Selected spectral data of some synthesized arylaminotetrazoles

1-(4-Nitrophenyl)-1*H*–tetrazole-5-amine (**2a**): M.p. 187–188 °C; FT-IR (KBr, cm^{-1}): 3389, 3302, 3124, 1651, 1611, 1598, 1577, 1523, 1506, 1466, 1348, 1315, 1296, 1131, 1108, 1074, 867, 858, 751, 690, 588, 506, 449; ^{1}H NMR (500 MHz, DMSO-d_6): δ_H = 8.43 (d, J = 7.2 Hz, 2H), 7.91 (d, J = 7.2 Hz, 2H), 7.19 (s, 2H); ^{13}C NMR (125 MHz, DMSO-d_6): δ_C = 154.9, 147.1, 138.6, 125.3, 124.6; Anal. Calcd for $C_7H_6N_6O_2$: C, 40.78; H, 2.93; N, 40.77; Found: C, 40.88; H, 3.01; N, 40.67.

N-(2-Chlorophenyl)-2*H*–tetrazole-5-amine (**2b**): M.p. 228–230 °C; FT-IR (KBr, cm^{-1}) 3329, 3157, 1660, 1595, 1578, 1499, 1460, 1317, 1130, 1081, 1040, 992, 760, 726, 712, 656, 559, 448; ^{1}H NMR (500 MHz, DMSO-d_6): δ_H = 14.86 (s, br, 1H), 9.12 (s, 1H), 8.00 (d, J = 8.2 Hz, 1H), 7.46 (d, J = 7.9 Hz, 1H), 7.33 (t, J = 8.4 Hz, 1H), 7.04 (t, J = 7.7 Hz, 1H); ^{13}C NMR (125 MHz, DMSO-d_6): δ_C = 154.8, 136.7, 129.6, 127.9, 123.5, 122.6, 120.2; Anal. Calcd for $C_7H_6N_5Cl$: C, 42.98; H, 3.09; N, 35.80. Found: C, 43.10; H, 3.19; N, 35.68.

TABLE 4 The most important second order perturbation energies (kcal/mole) for the acceptor–donor atoms of the Mn complex obtained from the NBO calculations

$\varepsilon_i - \varepsilon_j$	$E_{(2)}$	$F_{i,j}$	Acceptor	Donor	Structure
0.01	3.9	0.022	BD* (N10-Mn18)	BD (C11-C12)	Mn complex
0.01	3.9	0.022	BD* (N17-Mn18)	BD (C15-C16)	
0.65	0.39	0.020	BD* (C16-N17)	LP (2) Mn18	
0.61	1.35	0.036	BD* (C7-N17)	LP (2) Mn18	

N-(2,5-Dichlorophenyl)-2*H*–tetrazol-5-amine (**2c**): M.p. 272–274 °C; FT-IR (KBr, cm^{-1}) 3330, 3170, 1659, 1588, 1568, 1492, 1457, 1396, 1311, 1250, 1142, 1100, 1080, 1030, 989, 885, 825, 813, 757, 737, 689, 671, 590, 499, 482, 449; ^{1}H NMR (500 MHz, DMSO-d_6): δ_H = 14.72 (s, br, 1H), 9.38 (s, 1H), 8.19 (s, 1H), 7.48 (d, J = 8.5 Hz, 1H), 7.06 (d, J = 8.5 Hz, 1H); ^{13}C NMR (125 MHz, DMSO-d_6): δ_C = 154.4, 137.8, 132.3, 130.8, 122.5, 120.3, 118.7; Anal. Calcd for $C_7H_5N_5Cl_2$: C, 36.52; H,2.17; N, 30.43. Found: C, 36.66; H, 2.22; N, 30.56.

1-*p*-Tolyl-1*H*-tetrazol-5-amine (**2d**): M.p. 178–179 °C; FT-IR (KBr, cm^{-1}) 3310, 3146, 2920, 1655, 1594, 1572, 1519, 1466, 1321, 1306, 1287, 1180, 1141, 1091, 1017, 919, 889, 819, 765, 739, 709, 672, 636, 618, 545, 483; ^{1}H NMR (500 MHz, DMSO-d_6): δ_H = 7.43 (d, J = 8.2 Hz, 2H), 7.39 (d, J = 8.2 Hz, 2H), 6.80 (s, 2H), 2.38 (s, 3H); ^{13}C NMR (125 MHz, DMSO-d_6): δ_C = 155.8, 139.8, 131.8, 131.1, 124.8, 21.6.

1-*o*-Tolyl-1*H*-tetrazol-5-amine (**2e**): M.p. 191–192 °C; FT-IR (KBr, cm^{-1}) 3323, 3160, 1656, 1593,

1576, 1504, 1473, 1378, 1313, 1293, 1139, 1091, 1027, 994, 773, 758, 716, 674, 565, 486, 445; ^{1}H NMR (300 MHz, DMSO-d_6): δ_H = 7.51–7.36 (m, 4H), 6.74 (s, 2H), 2.06 (s, 3H).

1-(2,4-Dimethylphenyl)-1*H*–tetrazol-5-amine (**2f**): M.p. 199–201 °C; FT-IR (KBr, cm^{-1}) 3312, 3152, 1954, 2922, 1655, 1593, 1576, 1509, 1460, 1378, 1355, 1315, 1237, 1137, 1091, 1030, 1091, 997, 870, 829, 617, 565, 496, 444; ^{1}H NMR (500 MHz, DMSO-d_6): δ_H = 7.28 (s, 1H), 7.22 (d, J = 8.2 Hz, 1H), 7.19 (d, J = 8.2 Hz, 1H), 6.63 (s, 2H), 2.36 (s, 3H), 1.99 (s, 3H); ^{13}C NMR (125 MHz, DMSO-d_6): δ_C = 155.6, 140.0, 134.9, 131.7, 129.4, 127.6, 127.1, 20.6, 16.7.

1,1′-(1,4-Phenylene)bis(1*H*–tetrazol-5-amine) (**2 g**): M.p. 264–266 °C; FT-IR (KBr, cm^{-1}) 3321, 3145, 1659, 1587, 1522, 1447, 1427, 1325, 1292, 1142, 1120, 1088, 1019, 852, 843, 737, 651, 575; ^{1}H NMR (500 MHz, DMSO-d_6) δ_H = 7.83 (s, 4H), 7.03 (s, 4H); ^{13}C NMR (125 MHz, DMSO-d_6) δ_C = 155.9, 134.6, 126.3; Anal. Calcd for $C_8H_8N_{10}$: C, 39.35; H, 3.30; N, 57.35. Found: C, 39.46; H, 3.42; N, 57.23.

N-(4-Bromophenyl)-2*H*–tetrazol-5-amine (**2 h**): M.p. 249–250 °C; FT-IR (KBr, cm^{-1}): 3266, 3128, 3074, 1626, 1578, 1545, 1486, 1246, 1070, 1009, 835, 784, 728, 584, 500; ^{1}H NMR (300 MHz, DMSO-d_6): δ_H = 15.57 (s, br, 1H), 9.98 (s, br, 1H), 7.53–7.45 (m, 4H); ^{13}C NMR (75 MHz, DMSO-d_6): δ_C = 156.1, 140.3, 132.2, 119.2, 112.8; Anal. Calcd for $C_7H_6N_5Br$: C, 35.02; H, 2.52; N, 29.17. Found: C, 35.11; H, 2.64; N, 29.24.

1-(4-Chlorophenyl)-1*H*–tetrazol-5-amine (**2i**): M.p. 217–219 °C; FT-IR (KBr, cm^{-1}) 3351, 3147, 1651, 1593, 1578, 1499, 1410, 1325, 1143, 1095, 1075, 1011, 838, 820, 557, 514, 470; ^{1}H NMR (500 MHz, DMSO-d_6): δ_H = 7.68 (d, J = 8.6 Hz, 2H), 7.62 (d, J = 8.6 Hz, 2H), 6.94 (s, 2H); ^{13}C NMR (125 MHz, DMSO-d_6): δ_C = 155.8, 134.6, 133.2, 130.6, 126.9.

1-(4-Methoxyphenyl)-1*H*–tetrazol-5-amine (**2j**): M.p. 211–213 °C; FT-IR (KBr, cm^{-1}): 3282, 3194, 3068, 2962, 1622, 1588, 1542, 1512, 1467, 1307, 1243, 1187, 1109, 1056, 1034, 996, 831, 790, 767, 725, 675, 566, 521; ^{1}H NMR (500 MHz, acetone-d_6): δ_H = 7.49 (d, J = 8.9 Hz, 2H), 7.14 (d, J = 8.9 Hz, 2H), 6.14 (s, 2H), 3.89 (s, 3H); ^{13}C NMR (125 MHz, acetone-d_6): δ_C = 161.5, 156.2, 127.7, 127.1, 115.9, 56.19; Anal. Calcd for $C_8H_9N_5O$: C, 50.25; H, 4.74; N, 36.63. Found: C, 50.21; H, 4.81; N, 36.75.

1-(2,6-Dimethylphenyl)-1*H*–tetrazol-5-amine (**2 k**): M.p. 147–149 °C; FT-IR (KBr, cm^{-1}): 3441, 3383, 3351, 2952, 2921, 1697, 1651, 1604, 1583, 1558, 1526, 1486, 1442, 1247, 1228, 1194, 1168, 1032, 987, 938, 780; ^{1}H NMR (500 MHz, DMSO-d_6): δ_H = 7.03 (s, 3H), 5.24 (s, 2H), 2.25 (s, 6H); ^{13}C NMR (125 MHz, DMSO-d_6): δ_C = 157.5, 137.1, 136.6, 128.3, 126.3, 18.6; Anal.Calcd for $C_9H_{11}N_5$: C, 57.12; H, 5.86; N, 37.02. Found: C, 57.18; H, 5.90; N, 37.09.

4 | CONCLUSION

In conclusion, the Fe@Phendiol@Mn nano-catalyst was prepared, characterized by different methods and the Mn nano-catalyst used for the selective synthesis of various arylaminotetrazole derivatives (**A** or **B**).

Also, the theoretical study of the Fe@Phendiol@Mn nano-catalyst by the Gausian software showed that the complex is stable. In addition, some physicochemical parameters were calculated, and the big distance between the HOMO and LUMO levels indicated that the Mn complex is not a good conductive compound.

ACKNOWLEDGEMENTS

We are thankful to the Bu-Ali Sina University, Hamedan 6517838683 Iran, for the financial support of this work.

REFERENCES

[1] S. J. Wittenberger, *Org. Prep. Proceed. Int.* **1994**, *26*, 499.

[2] R. N. Bulter, in *Comprehensive Heterocyclic Chemistry II*, (Eds: A. R. Katritzky, C. W. Rees, E. F. V. Scriven), Pergamon, New York, NY **1996** Vol. *4*,621.

[3] R. J. Herr, *Bioorg. Med. Chem.* **2002**, *10*, 3379.

[4] N. P. Peet, L. E. Baugh, S. Sundler, J. E. Lewis, E. H. Matthews, E. L. Olberding, D. N. Shah, *J. Med. Chem.* **1986**, *29*, 2403.

[5] V. M. Girijavallabhan, P. A. Pinto, A. K. Genguly, R. W. Versace, Eur. Patent **1988**, EP 274867 *Chem. Abstr.* 1989, *110*, 23890.

[6] H. Akimoto, K. Ootsu, F. Itoh, Eur. Patent EP 530537, **1993**; *Chem. Abstr.* 1993, *119*, 226417.

[7] C. H. Mitch, S. J. Quimby, Int. Patent WO 9851312, **1998**; *Chem. Abstr.* 1998, *130*, 13997.

[8] B. S. Jursic, B. W. LeBlanc, *J. Heterocycl. Chem.* **1998**, *35*, 405.

[9] E. O. John, R. L. Kirchmeier, J. M. Shreeve, *Inorg. Chem.* **1989**, *28*, 4629.

[10] C. Zhao-Xu, X. Heming, *Int. J. Quantum Chem.* **2000**, *79*, 350.

[11] F. Ek, L.-G. Wistrand, T. Frejd, *Tetrahedron* **2003**, *59*, 6759.

[12] L. A. Flippin, *Tetrahedron Lett.* **1991**, *32*, 6857.

[13] P. Rhonnstad, D. Wensbo, *Tetrahedron Lett.* **2002**, *43*, 3137.

[14] A. R. Modarresi-Alam, F. Khamooshi, M. Rostamizadeh, H. Kieykha, M. Nasrollahzadeh, H. R. Bijanzadeh, E. Kleinpeter, *J. Mol. Struct.* **2007**, *841*, 67.

[15] G. Sandmann, C. Schneider, P. Boger, *Z. Naturforsch. C. Biosci.* **1996**, *51*, 534.

[16] B. S. Jursic, B. W. Leblanc, *J. Heterocycl. Chem.* **1998**, *35*, 405.

[17] C. Zhao-Xu, X. Heming, *Int. J. Quantum Chem.* **2000**, *79*, 350.

[18] R. N. Bulter, in *Comprehensive heterocyclic chemistry II*, (Eds: A. R. Katritzky, C. W. Rees, E. F. V. Scriven) Vol. 4, Oxford, Pergamon **1996**.

[19] C. Hansch, L. Leo, *Exploring QSAR, Fundamentals and Applications in Chemistry and Biology*, American Chemical Society, Washington, DC **1995** Chapter 13.

[20] R. N. Butler, *Adv. Heterocycl. Chem.* **1977**, *21*, 323.

[21] S. J. Wittenberger, *Org. Prep. Proceed. Int.* **1994**, *26*, 499.

[22] R. J. Herr, *Bioorg. Med. Chem.* **2002**, *10*, 3379.

[23] A. R. Modarresi-Alam, F. Khamooshi, M. Rostamizadeh, H. Kieykha, M. Nasrollahzadeh, H. R. Bijanzadeh, E. Kleinpeter, *J. Mol. Struct.* **2007**, *841*, 67.

[24] P. K. Kadaba, *Synthesis* **1973**, 71.

[25] A. R. Katritzky, B. V. Rogovoy, K. V. Kovalenko, *J. Org. Chem.* **2003**, *68*, 4941.

[26] M. L. Kantam, K. B. Shiva Kumar, C. Sridhar, *Adv. Synth. Catal.* **2005**, *347*, 1212.

[27] W. L. Garbrecht, R. M. Herbst, *J. Org. Chem.* **1953**, *18*, 1014.

[28] W. G. Finnegan, R. A. Henry, E. Lieber, *J. Org. Chem.* **1953**, *18*, 779.

[29] R. A. Henry, W. G. Finnegan, E. Lieber, *J. Am. Chem. Soc.* **1955**, *77*, 2264.

[30] W. L. Garbrecht, R. M. Herbst, *J. Org. Chem.* **1953**, *18*, 1014.

[31] V. J. Braun, *Chem. Ber.* **1900**, *33*, 1438.

[32] R. N. Butler, *Adv. Heterocycl. Chem.* **1977**, *21*, 323.

[33] S. J. Wittenberger, *Org. Prep. Proceed. Int.* **1994**, *26*, 499.

[34] R. J. Herr, *Bioorg. Med. Chem.* **2002**, *10*, 3379.

[35] B. S. Jursic, B. W. Leblanc, *J. Heterocycl. Chem.* **1998**, *35*, 405.

[36] T. Jin, F. Kitahara, S. Kamijo, Y. Yamamoto, *Tetrahedron Lett.* **2008**, *49*, 2824.

[37] M. S. Congreve, *Synlett* **1996**, 359.

[38] A. N. Vorobiev, P. N. Gaponik, P. T. Petrov, Vestsi Nats. Akad. Navuk Belarusi, Ser. Khim. Navuk **2003**, 50; *Chem. Abstr.* 2004, *140*, 16784g.

[39] M. Nasrollahzadeh, D. Habibi, A. Faraji, Y. Bayat, *Tetrahedron* **2010**, *66*, 3866.

[40] D. Habibi, M. Nasrollahzadeh, Y. Bayat, *Synth. Commun.* **2011**, *41*, 2135.

[41] M. Nasrollahzadeh, D. Habibi, Z. Shahkarami, Y. Bayat, *Tetrahedron* **2009**, *65*, 10715.

[42] D. Azarifar, D. Sheikh, *Synth. Commun.* **2013**, *43*, 2517.

[43] V. Ponec, G. C. Bond, *Catalysis by Metals and Alloys*, Elsevier, Amsterdam **1996**.

[44] C. W. Lim, I. S. Lee, *Nano Today* **2010**, *5*, 412.

[45] D. Habibi, S. Heydari, A. Gil, M. Afsharfarnia, A. Faraji, M. Asadbegy, R. Karamian, **2016**, Submitted, under review.

[46] M. Yamada, Y. Tanaka, Y. Yoshimoto, S. Kuroda, I. Shimao, *Bull. Chem. Soc. Jpn.* **1992**, *65*, 1006.

[47] T. S. Bruice, T. C. Eckert, *J. Am. Chem. Soc.* **1983**, *105*, 4431.

[48] H. W. Nesbitt, D. Banerjee, *Am. Mineral.* **1998**, *83*, 305.

[49] D. Habibi, M. Nasrollahzadeh, *Synth. Commun.* **2010**, *40*, 3159.

[50] J. P. Hay, R. W. Wadt, *J. Chem. Phys.* **1985**, *82*, 270.

[51] M. W. Schmidt, K. K. Baldridge, J. A. Boatz, S. T. Elbert, M. S. Gordon, J. H. Jensen, S. Koseki, N. Matsunaga, K. A. Nguyen, S. J. Su, T. L. Windus, M. Dupuis, J. A. Montgomery, *J. Comput. Chem.* **1993**, *14*, 1347.

[52] P. K. Chattaraj, U. Sarkar, D. R. Roy, *Chem. Rev.* **2006**, *106*, 2065.

[53] K. K. Hazarika, N. C. Baruah, R. C. Deka, *Struct. Chem.* **2009**, *20*, 1079.

[54] R. G. Parr, L. Szentpaly, S. Liu, *J. Am. Chem. Soc.* **1999**, *121*, 1922.

[55] G. Mehta, G. Gunasekaran, S. R. Gadre, R. N. Shirsat, B. Ganguly, J. Chandrasekhar, *J. Org. Chem.* **1994**, *59*, 1953.

[56] J. K. Badenhoop, F. Weinhold, *Int. J. Quantum Chem.* **1999**, *72*, 269.

SUPPORTING INFORMATION

Additional Supporting Information may be found online in the supporting information tab for this article.

How to cite this article: Habibi D, Heydari S, Afsharfarnia M, Rostami Z. A versatile synthesis of arylaminotetrazoles by a magnetic Fe@Phendiol@Mn nano-particle catalyst and its theoretical studies. *Appl Organometal Chem*. 2017:e3826. https://doi.org/10.1002/aoc.3826